Molecular Crystals and Liquid Crystals

ISSN: 1542-1406 (Print) 1563-5287 (Online) Journal homepage: http://www.tandfonline.com/loi/gmcl20

Synthesis, X-ray Structure and Spectroscopic Properties of 7,9-Diiodobenzo[h]quinolin-10-ol

Kew-Yu Chen

To cite this article: Kew-Yu Chen (2015) Synthesis, X-ray Structure and Spectroscopic Properties of 7,9-Diiodobenzo[h]quinolin-10-ol, Molecular Crystals and Liquid Crystals, 616:1, 202-212, DOI: 10.1080/15421406.2014.991129

To link to this article: http://dx.doi.org/10.1080/15421406.2014.991129

Mol. Cryst. Liq. Cryst., Vol. 616: pp. 202–212, 2015

ISSN: 1542-1406 print/1563-5287 online
DOI: 10.1080/15421406.2014.991129

Synthesis, X-ray Structure and Spectroscopic Properties of 7,9-Diiodobenzo[*h*]quinolin-10-ol

KEW-YU CHEN*

Department of Chemical Engineering, Feng Chia University, Taichung, Taiwan, ROC

*7,9-Diiodobenzo[*h*]quinolin-10-ol (**1**), a benzo[*h*]quinolin-10-ol derivative, was synthesized and characterized by single-crystal X-ray diffraction. The crystal belongs to monoclinic, space group* $P2_1/c$, *with* $a = 7.3765(16)$, $b = 12.616(2)$, $c = 12.881(2)$ Å, $\alpha = 90^\circ$, $\beta = 93.420(16)^\circ$, *and* $\gamma = 90^\circ$. *Compound **1** possesses an intramolecular six-membered-ring hydrogen bond, from which excited-state intramolecular proton transfer takes place, resulting in a proton-transfer tautomer emission of 628 nm in cyclohexane. Moreover, the geometric structures, frontier molecular orbitals and the potential energy curves for **1** in the ground and the first singlet excited state were fully rationalized by density functional theory (DFT) and time-dependent DFT calculations.*

Keywords Benzo[*h*]quinolin-10-ol; DFT calculations; ESIPT; X-ray diffraction; 7,9-Diiodobenzo[*h*]quinolin-10-ol

1. Introduction

The excited-state intramolecular proton transfer (ESIPT) reaction of benzo[*h*]quinolin-10-ol (**2**) has been investigated [1] using the femtosecond fluorescence up-conversion technique. As shown in Fig. 1, the ESIPT reaction involves transfer of a hydroxyl proton to an imine nitrogen through an intramolecular six-membered-ring hydrogen-bonding configuration [2–6]. The resulting proton-transfer tautomer (keto-form) possesses considerable differences in structure and electronic configuration from its corresponding ground state, *i.e.*, a large Stokes shifted $K^* \rightarrow K$ fluorescence. This unusual optical property has found many important applications such as probes for solvation dynamics [7–9] and biological environments [10,11], photochromic materials [12], fluorescence microscopy imaging [13], nonlinear optical materials [14], near-infrared fluorescent dyes [15], organic light-emitting diodes [16–20], and chemosensors [21–25]. In an effort to expand the scope of **2**-based chromophores available for designing systems for fluorescent dyes and optoelectronic materials, the present research reports the synthesis of a benzo[*h*]quinolin-10-ol derivative 7,9-Diiodobenzo[*h*]quinolin-10-ol (**1**) as well as its X-ray structure, photophysical properties and complementary time-dependent density functional theory (TD-DFT) calculations. The results offer the potential to synthesize benzo[*h*]quinolin-10-ol derivatives with extended molecular architectures and optical properties.

*Address correspondence to Kew-Yu Chen, Department of Chemical Engineering, Feng Chia University 40724, Taichung, Taiwan, ROC. E-mail: kyuchen@fcu.edu.tw

Color versions of one or more of the figures in the article can be found online at www.tandfonline.com/gmcl.

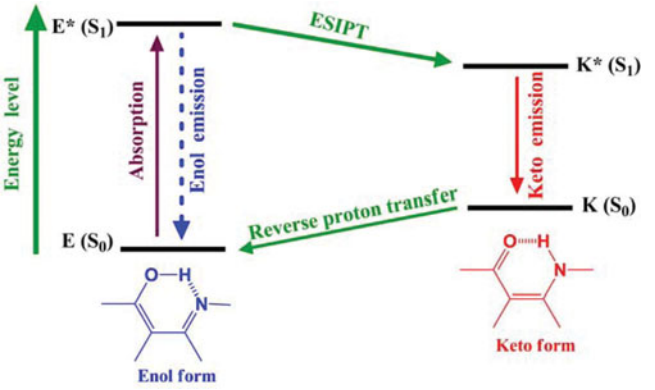

Figure 1. Characteristic four-level photocycle scheme of the ESIPT process.

2. Experimental

2.1. Chemicals and Instruments

The starting materials such as benzo[*h*]quinolin-10-ol (**2**), iodine, acetic acid, and dichloromethane were purchased from Merck, ACROS and Sigma–Aldrich. Column chromatography was performed using silica gel Merck Kieselgel *si* 60 (40–63 mesh).

^{1}H NMR spectra were recorded in $CDCl_3$ on a Bruker 400 MHz. Mass spectra were recorded on a VG70-250S mass spectrometer. The absorption and emission spectra were measured using a Jasco V-570 UV–Vis spectrophotometer and a Hitachi F-4500 fluorescence spectrophotometer, respectively. The single-crystal X-ray diffraction data were collected on a Bruker Smart 1000CCD area-detector diffractometer.

2.2. Synthesis and Characterization

*2.2a. Synthesis of **1**.* A solution containing benzo[*h*]quinolin-10-ol (195 mg, 1.0 mmol) and acetic acid (1.0 mL) in dichloromethane (30 mL) to a solution of iodine (680 mg, 2.7 mmol in 30 mL methanol) for a period of 1 hr. The reaction mixture was refluxed for 6 h. After cooling, the mixture was neutralized with 10% KOH and extracted with CH_2Cl_2 (3 × 25 mL). After solvent was removed, the crude product was purified by silica gel column chromatography with eluent ethyl acetate/*n*-hexane (1/4) to afford **1** (410 mg, 92%). ^{1}H NMR (400 MHz, $CDCl_3$, in ppm) δ 16,73 (s, 1H, H_7), 8.89 (dd, $J_1 = 4.6$ Hz, $J_2 = 1.6$ Hz, H_1), 8.59 (s, H_6), 8.38 (dd, $J_1 = 8.1$ Hz, $J_2 = 1.6$ Hz, H_3), 8.13 (d, $J = 9.2$ Hz, H_5), 7.80 (d, $J = 9.2$ Hz, H_4), 7.69 (dd, $J_1 = 8.1$ Hz, $J_2 = 4.6$ Hz, H_2); MS (EI, 70eV): *m/z* (relative intensity) 446 (M^+, 100); HRMS calcd. for $C_{13}H_7I_2NO$ 446.8617, found 446.8611. Orange parallelepiped-shaped crystals suitable for the crystallographic studies reported here were isolated over a period of 5 weeks by slow evaporation from a dichloromethane solution.

2.2b. Crystal Structural Determination. A single crystal of the title compound with dimensions of 0.30 mm × 0.20 mm × 0.16 mm was selected. The lattice constants and diffraction

intensities were measured with a Bruker Smart 1000CCD area detector radiation (λ = 0.71073 Å) at 110.0(2) K. An ω-2θ scan mode was used for data collection in the range of $3.10 \leqq \theta \leqq 29.16^{\circ}$. A total of 5626 reflections were collected and 2762 were independent ($R_{int} = 0.0438$), of which 2298 were considered to be observed with $I > 2\sigma(I)$ and used in the succeeding refinement. The structure was solved by direct methods with SHELXS-97 [26] and refined on F^2 by full-matrix least-squares procedure with Bruker SHELXL-97 packing [27]. All nonhydrogen atoms were refined with anisotropic thermal parameters. The hydrogen atoms refined with riding model position parameters isotropically were located from difference Fourier map and added theoretically. At the final cycle of refinement, $R = 0.0639$ and $wR = 0.1644$ ($w = 1/[\sigma^2(F_o^2) + (0.0859P)^2 + 7.8496P]$, where $P = (F_o^2 + 2F_c^2)/3$). $S = 1.124$, $(\Delta/\sigma)_{max} = 0.001$, $(\Delta/\rho)_{max} = 3.932$, and $(\Delta/\rho)_{min} = —1.923$ e/Å^3 were observed. Crystallographic data for the structure reported in this article have been deposited in the Cambridge Crystallographic Data Center with a supplementary publication number of CCDC 1019569. Copies of these information can be obtained free of charge from the Director, CCDC, 12 Union Road, Cambridge CB2 1EZ, UK (fax: +44 1223 336 033; e-mail: deposit@ccdc.cam.ac.uk).

2.3. *Computational Methods*

The Gaussian 03 program was used to perform the ab initio calculation on the molecular structure [28]. Geometry optimization for compound **1** was carried out with the LanL2DZ basis set to the B3LYP functional. Vibrational frequencies were also performed to check whether the optimized geometrical structures for both compounds were at energy minima, transition states, or higher order saddle points. After obtaining the converged geometries, the TD-B3LYP/LanL2DZ was used to calculate the vertical excitation energy, and the emission energy was obtained from TDDFT/B3LYP/LanL2DZ calculations performed on S_1 optimized geometries.

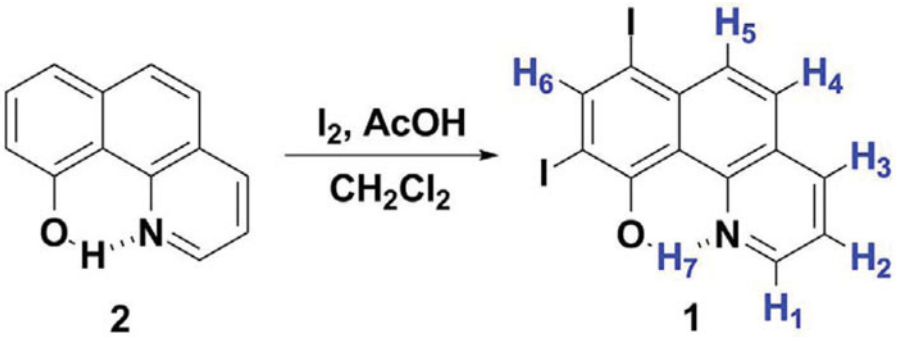

Scheme 1. The synthetic route and the structure for **1**. The Non-IUPAC atom label is for the convenience of ^{1}H NMR assignment.

3. Results and Discussion

Scheme 1 shows the synthetic route and the chemical structure of **1**. The iodination of **2** was carried out by the reaction of **2** with iodine in the presence of acetic acid, giving **1** in a good yield of 92% after purification. The structure of 7,9-diiodobenzo[*h*]quinolin-10-ol (**1**) can be verified by the presence of only seven signals (two singlet and two doublet signals,

Table 1. Crystallographic data for compounds **1** and **2**

Compound	1	2
Chemical formula	$C_{13}H_7I_2NO$	$C_{13}H_9NO$
Formula weight	447.00	195.21
Crystal system	Monoclinic	Orthorhombic
Space group	$P2_1/c$	$Pbc2_1$
a (Å)	7.3765(16)	4.6530(4)
b (Å)	12.616(2)	15.1910 (10)
c (Å)	12.881(2)	26.902 (2)
α (°)	90	90
β (°)	93.420(16)	90
γ (°)	90	90
Volume (Å^3)	1196.6(4)	1901.5(2)
Z	4	8
D_{calc} (g cm^{-3})	2.481	1.364
μ (mm^{-1})	5.237	0.695
F_{000}	824	816
Crystal size (mm^3)	0.30 × 0.20 × 0.16	0.35 × 0.20 × 0.15
θ range (°)	3.10–29.16	19.35–37.54
Index ranges	$-9 \leqq h \leqq 9$	$0 \leqq h \leqq 5$
	$-17 \leqq k \leqq 15$	$0 \leqq k \leqq 16$
	$-17 \leqq l \leqq 15$	$0 \leqq l \leqq 29$
Reflections collected	5626	1312
Independent reflections (R_{int})	2762 (0.0438)	1312 (0.0000)
Refinement method on F^2	Full-matrix least-squares	Full-matrix least-squares
GOF on F^2	1.124	1.213
R_1 [$I > 2\sigma$ (I)]	0.0639	0.0383
wR_2 [$I > 2\sigma$ (I)]	0.1644	0.0767
R_1 (all data)	0.0767	0.0559
wR_2 (all data)	0.1739	0.1128
Residual (e Å^{-3})	3.932 and –1.923	0.117 and –0.131

and three doublet of doublets signals) at δ 7.5–17.0 ppm in the ^{1}H NMR spectrum, which indicates that the iodination at the 7,9- positions of **2** was achieved. The detailed assignment of each proton was also carried out through chemical shift and coupling constant (see 2.2a). To confirm its structure, a single crystal of **1** was obtained from a dichloromethane solution, and the molecular structure was determined by X-ray diffraction analysis. In addition, its X-ray structure is compared with that of **2** [29].

The dominance of an enol-form for **1** and **2** is supported by a combination of ^{1}H NMR and X-ray single-crystal analyses. In the ^{1}H NMR studies, the existence of a strong hydrogen bond between O–H and N is evidenced by the observation of a large downfield shift of the proton peak at $\delta > 14$ ppm (in dry $CDCl_3$) for both compounds **1** (16.73 ppm) and **2** (14.86 ppm). According to Schaefer's equation [30], the hydrogen bonding energy (ΔE in kcal/mol) of **1** and **2** can be calculated to be as large as 12.84 ± 0.2 kcal/mol and 10.97 ± 0.2 kcal/mol, respectively. Note that the substitution of the hydrogen atoms at the

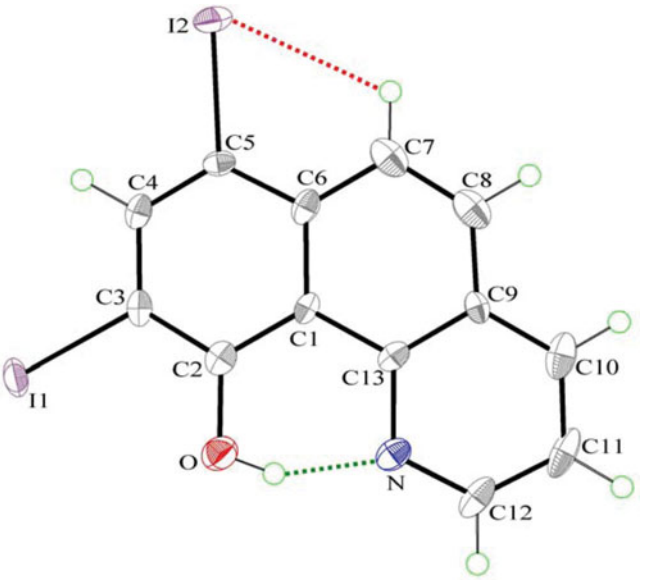

Figure 2. The molecular structure of **1**, showing the atom-labeling scheme. Displacement ellipsoids are drawn at the 50% probability level. Green and red dashed lines denote the intramolecular O—H···N and C—H···I hydrogen bonds.

7,9-positions in **2** by iodine atoms, forming **1**, seems to increase the acidity of phenol (O–H) through an inductive effect. As a result, **1** shows a downfield shift of the O–H proton, and hence, a stronger hydrogen bond relative to **2**.

Compound **1** crystallizes in the space group $P2_1/c$ with $Z' = 1$, whereas the closely related compound **2** crystallizes with $Z' = 2$ in the space group $Pbc2_1$ (Table 1). Figure 2 shows the *ORTEP* diagram of **1**. The complete molecule is nearly planar, as indicated by the key torsion angles (Table 2). The maximum deviations from the mean plane through the non-H atoms are 0.077(1) Å for atom I(1) and 0.078(1) Å for atom I(2). The dihedral angle between the terminal ring planes is 1.0(2)°, which is slightly smaller than that in **2** (2.3(2)°). Compound **1** possesses an intramolecular O–H···N hydrogen bond [31–34], which generates an S(6) ring motif. The dihedral angle between the mean plane of the S(6) ring and the mean plane of the pyridine ring is 0.66(2)°. This, together with 2.501(12) Å of O(1)···N distance and 150° of O(1)–H(0A)···N, strongly supports the S(6) ring formation. The parameters of the hydrogen bond of **1** (Table 3) are slightly different from those of **2** (2.562(5) Å of O(1)···N distance and 138(3)° of O(1)–H(0A)–N). Furthermore, there is a weak intramolecular C–H···I hydrogen bond in **1** (3.270(12) Å of C(7)···I(2) distance and 112° of C(7)–H(7A)–I(2), Table 3), which generates another S(5) motif. In good agreement with these observations, the ^{1}H NMR spectrum (in $CDCl_3$) revealed a significantly downfield signal at δ 8.13 ppm (H_5, see 2.2a), giving a clear indication of the five-membered ring intramolecular hydrogen bond formation. The bond-length and angle patterns of **1** are typical, the long C(1)–C(6) bond (1.459(13) Å) and the short C(9)–C(13) bond (1.383(13) Å) support the results of the studies on *o*-phenanthroline [35].

Figure 3 shows the molecular packing of **1** in the crystal unit cell. The crystal structure is stabilized by intermolecular π–π interactions, which links a pair of molecules into a cyclic centrosymmetric dimer. Pertinent measurements for these $\pi\cdots\pi$ interactions are:

Table 2. Comparison of the experimental and optimized geometric parameters of **1** (Å and °)

	X-ray	DFT
Bond lengths (Å)		
O(1)-C(2)	1.370(12)	1.362
N-C(12)	1.341(12)	1.342
N-C(13)	1.402(12)	1.380
C(1)-C(6)	1.459(13)	1.439
C(9)-C(13)	1.383(13)	1.403
C(11)-C(12)	1.383(15)	1.395
I(1)-C(3)	2.092(9)	2.122
I(2)-C(5)	2.095(9)	2.149
Bond angles (°)		
C(12)-N-C(13)	116.9(9)	119.1
O-C(2)-C(3)	120.8(9)	120.0
C(1)-C(2)-C(3)	118.4(9)	118.9
C(4)-C(5)-C(6)	122.1(9)	120.9
C(10)-C(9)-C(13)	119.2(9)	118.2
C(10)-C(11)-C(12)	116.0(9)	118.6
Torsion angles (°)		
C(13)-N-C(12)-C(11)	–0.4(13)	–0.1
O-C(2)-C(3)-I(1)	–1.6(12)	–0.1
C(1)-C(2)-C(3)-C(4)	–1.9(13)	–0.1
C(6)-C(1)-C(13)-C(9)	1.1(13)	0.1

centroid–centroid distances of 3.581(5) (black dashed lines, symmetry code: 1–X, –Y, 1–Z), 3.654(6) (blue dashed lines, symmetry code: 1–X, –Y, 1–Z), 3.802(5) (red dashed lines, symmetry code: –X, –Y, 1–Z), and 3.578(5) Å (green dashed lines, symmetry code: –X, –Y, 1–Z). These $\pi\cdots\pi$ interactions lead to the formation of columns along the [100] direction that are connected to one another *via* intermolecular I(1)···I(1) (3.7036(12) Å, pink dashed lines, symmetry code: –X, –Y, –Z) and I(2)···I(2) (3.6677(12) Å, orange dashed lines, symmetry code: –X, 1–Y, 1–Z) contacts, so linking the molecules into a continuous three-dimensional framework.

Figure 4 shows the steady state absorption and emission spectra of **1** in cyclohexane. The lowest energy absorption band of **1** appears at 377 nm, which is assigned to the $\pi-\pi^*$ transition (vide infra). Another higher energy absorption band is also observed at 315 nm. As for the steady-state emission, compound **1** exhibits solely a long wavelength emission at 628 nm in cyclohexane (excitation at 375 nm). Figure 4 also depicts a large

Table 3. Hydrogen-bond geometry (Å, º)

D—H···*Cg*	d(D—H)	d(H···*Cg*)	d(D···*Cg*)	∠DH*Cg*
O–H(0A)···N	0.84	1.74	2.501(12)	150
C(7)–H(7A)···I(2)	0.95	2.80	3.270(12)	112

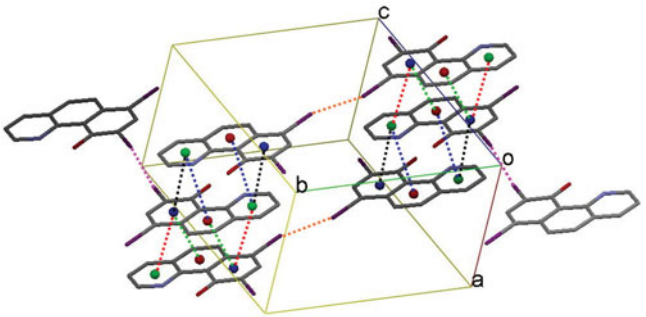

Figure 3. Part of the crystal structure in the unit cell of **1**, showing the formation of the dimmer built from $\pi\cdots\pi$ interactions. *C*g1 (green circles), *C*g2 (blue circles), and *C*g3 (red circles) are the centroids of the C9–C13/N, C1–C6, and C1/C6–C9/C13 rings, respectively. Black, blue, red, and green dashed lines denote four different intermolecular $\pi\cdots\pi$ interactions, respectively. Pink and orange dashed lines denote intermolecular I(1)···I(1) and I(2)···I(2) contacts. All hydrogen atoms are omitted for clarity.

separation of the energy gap between the 0 and 0 onset of the absorption and emission. The Stokes shift of the emission, defined by peak (absorption)-to-peak (emission) gap in terms of frequency, is calculated to be as large as 10602 cm^{-1}. Accordingly, the assignment of 628 nm in cyclohexane to a proton-transfer tautomer emission is unambiguous, and ESIPT takes place from the phenolic proton O–H(0A) to the pyridinic nitrogen, forming the keto-amine tautomeric species. The lack of any enol-normal emission in a steady state indicates that the ESIPT reaction is a barrierless process, which is strongly supported by the theoretical calculations (vide infra).

To gain deeper insight into the molecular structure and electronic properties of **1**, quantum chemical calculations were performed using density functional theory (DFT) at the B3LYP/LanL2DZ level. The geometric parameters (bond lengths, bond angles, and torsion angles) were compared with experimental data (Table 1). One can clearly see that

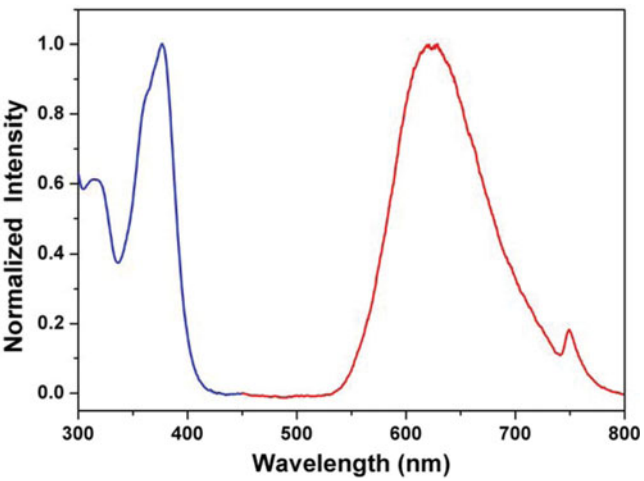

Figure 4. Normalized absorption (blue line) and emission (red line) spectra of **1** in cyclohexane.

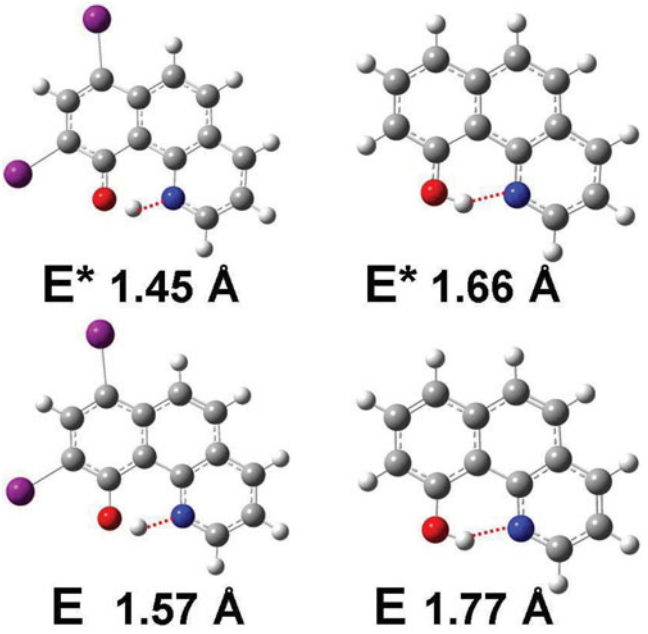

Figure 5. The optimized geometric structures of enol (E) form for **1** (left) and **2** (right) in the ground (S_0) and the first singlet excited state (S_1) together with the intramolecular hydrogen bond lengths. Red dashed lines denote the intromolecular O—H···N hydrogen bonds.

there are no obvious differences between the experimental and DFT/B3LYP calculated geometric parameters. Consequently, we can conclude that basis set LanL2DZ is suited in its approach to the experimental results.

The optimized geometric structures and the corresponding hydrogen bond lengths of enol form for **1** and **2** in the ground (S_0) and the first singlet excited state (S_1) are shown in Fig. 5. From E to E*, we can see that the intramolecular hydrogen bond length (red dashed lines) decreases from 1.57 (1.77) Å to 1.45 (1.66) Å for **1** (**2**). The results clearly provide the evidence for the strengthening of the intramolecular hydrogen bond from $S_0 \rightarrow S_1$. Therefore, there is no question that the decrease of intramolecular hydrogen bond lengths from E to E* is a very significant positive factor for the ESIPT reaction.

Figure 6 shows the HOMO and LUMO of enol and keto form of **1**. It can be observed that the first excited states for both enol and keto forms are a dominant $\pi \rightarrow \pi^*$ transition from the HOMO to the LUMO. Figure 6 also reveals that the electron density around the intramolecular hydrogen binding site is mainly populated at hydroxyl oxygen and pyridinic nitrogen at HOMO and LUMO, respectively. The results clearly demonstrate that upon electronic excitation of **1**, the hydroxyl proton (O–H) is expected to be more acidic, whereas the pyridinic nitrogen is more basic with respect to their ground state, driving the proton transfer reaction. In addition, the absorption and emission spectra of **1** were calculated by time-dependent DFT (TD-DFT) calculations (Franck–Condon principle). The calculated excitation (fluorescence) wavelength for the $S_0 \rightarrow S_{1\text{-}}$ ($S_1 \rightarrow S_0$) transition is 400 (638) nm, which is very close to the experimental results.

To explain the ESIPT properties of compounds **1** and **2**, the potential energy curves of the intramolecular proton transfer (i.e., the transformation from the enol form to the keto form) at both the ground state and the excited state were studied (Fig. 7). The full

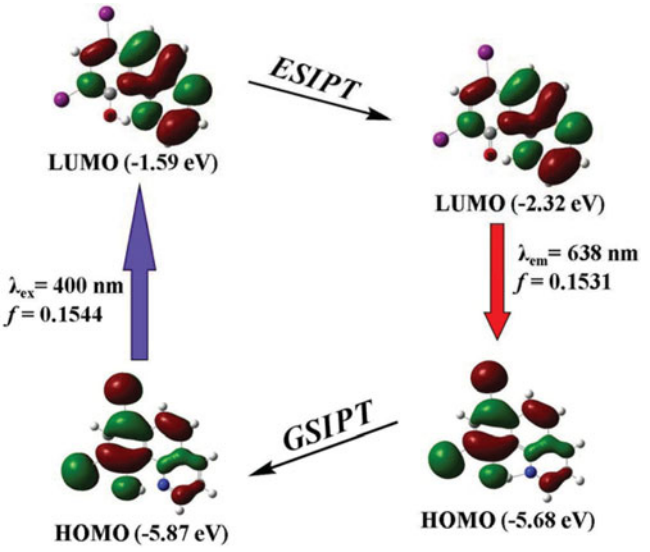

Figure 6. Selected frontier molecular orbitals involved in the excitation and emission of **1**.

geometry optimization based on the B3LYP/6-31G** theoretical level reveals that the normal form of **1** (**2**) in the ground state is more stable than the tautomeric form of **1** (**2**) by 5.1 (10.0) kcal/mol. It is apparent that the increased phenolic (O–H) acidity lowers the tautomerization energy by stabilizing the tautomers due to inductive effect of nearby iodine atom I(1). However, further calculations show that the corresponding proton-transfer tautomer is lower in energy than the respective **1** (**2**) by 15.7 (16.1) kcal/mol in the excited state. The results clearly demonstrate that ESIPT for both compounds is thermodynamically

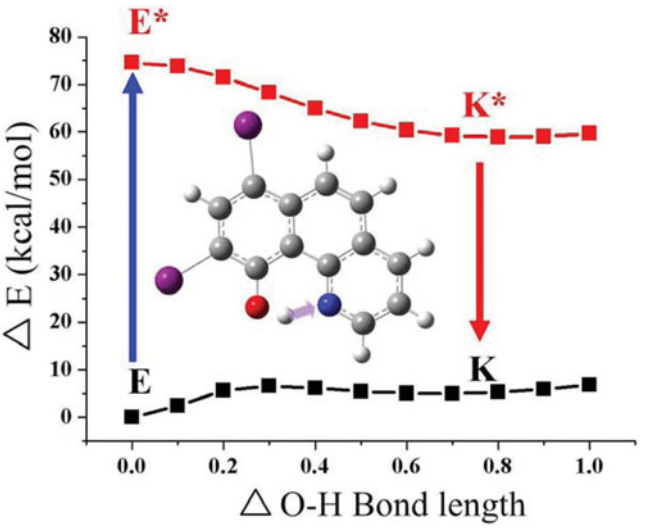

Figure 7. Potential energy curves from enol form to keto form of **1** at the ground state and excited state.

favorable, which are consistent with the experimental results. It is interesting to be noted that the comparison between the tautomerization energies of **1** and **2** does not show any substantial difference in the excited state.

4. Conclusions

A benzo[*h*]quinolin-10-ol derivative, namely, 7,9-diiodobenzo[*h*]quinolin-10-ol (**1**) was synthesized and fully characterized. Compound **1** possesses an intramolecular six-membered-ring hydrogen bond, from which ESIPT takes place, resulting in a proton-transfer tautomer emission of 628 nm in cyclohexane. The geometric structures, frontier molecular orbitals (MOs) and the potential energy curves for **1** in the ground and the first singlet excited state were fully rationalized by density functional theory (DFT) and time-dependent DFT calculations, and were in good agreement with the experimental results. Moreover, the single-crystal X-ray structure determinations described here have brought to light many interesting properties between **1** and **2** in the solid phase, including $\pi\cdots\pi$ stacking and inter- and intramolecular hydrogen bonding interactions. This offers the potential for synthesizing benzo[*h*]quinolin-10-ol derivatives with extended molecular architectures and optical properties.

Acknowledgments

The project was supported by the National Science Council (MOST 103-2113-M-035-001) and Feng Chia University in Taiwan. The authors appreciate the Precision Instrument Support Center of Feng Chia University for providing the fabrication and measurement facilities.

References

[1] Chou, P. T., & Wei, C. Y. (1996). *J. Phys. Chem.*, *100*, 17059.
[2] Chen, K. Y., Hsieh, C. C., Cheng, Y. M., Lai, C. H., & Chou, P. T. (2006). *Chem. Commun.*, *42*, 4395.
[3] Satam, M. A., Raut, R. K., Telore, R. D., & Sekar, N. (2013). *Dyes Pigm.*, *97*, 32.
[4] Luo, M. H., Tsai, H. Y., Lin, H. Y., Fang, S. Y., & Chen, K. Y. (2012). *Chin. Chem. Lett.*, *23*, 1279.
[5] Fang, T. C., Tsai, H. Y., Luo, M. H., Chang, C. W., & Chen, K. Y. (2013). *Chin. Chem. Lett.*, *24*, 145.
[6] Satam, M. A., Raut, R. K., & Sekar, N. (2013). *Dyes Pigm.*, *96*, 92.
[7] Chen, W. H., & Pang, Y. (2010). *Tetrahedron Lett.*, *51*, 1914.
[8] Xie, L., *et al.* (2012). *Dyes Pigm.*, *92*, 1361.
[9] Mahapatra, A. K., Mait, i. K., Sahoo, P., & Nandi, P. K. (2013). *J. Lumin.*, *143*, 349.
[10] Lim, C. K., *et al.* (2011). *Dyes Pigm.*, *90*, 284.
[11] Maupin, C. M., *et al.* (2011). *J. Am. Chem. Soc.*, *133*, 6223.
[12] Ito, Y., Amimoto, K., & Kawato, T. (2011). *Dyes Pigm.*, *89*, 319.
[13] Santos, R. C., *et al.* (2011). *Tetrahedron Lett.*, *52*, 3048.
[14] Ashraf, M., *et al.* (2012). *Dyes Pigm.*, *95*, 455.
[15] Ikeda, S., *et al.* (2010). *J. Org. Chem.*, *75*, 8637.
[16] Li, Y., *et al.* (2012). *J. Lumin.*, *132*, 1010.
[17] Chuang, W. T., *et al.* (2011). *J. Org. Chem.*, *76*, 8189.
[18] Xu, H., *et al.* (2012). *J. Lumin.*, *132*, 919.
[19] Tang, K. C., *et al.* (2011). *J. Am. Chem. Soc.*, *133*, 17738.

[20] Fang, S. K., Tsai, H. Y., Hu, J. W., & Chen, K. Y. (2014). *Int. J. Photoenergy*, 2014, Article ID 124753, 9 pages. doi:10.1155/2014/124753
[21] Hong, W. H., Lin, C. C., Hsieh, T. S., & Chang, C. C. (2012). *Dyes Pigm.*, *94*, 371.
[22] Huang, Q., Yang, X. F., & Li, H. (2013). *Dyes Pigm.*, *99*, 871.
[23] Prabhu, S., Saravanamoorthy, S., Ashok, M., & Velmathi, S. (2012). *J. Lumin.*, *132*, 979.
[24] Patil, V. S., Padalkar, V. S., Tathe, A. B., & Sekar, N. (2013). *Dyes Pigm.*, *98*, 507.
[25] Lin, W. C., Fang, S. K., Hu, J. W., Tsai, H. Y., & Chen, K. Y. (2014). *Anal. Chem.*, *86*, 4648.
[26] Sheldrick, G. M. (1997). *SHELXS97, A Program for Automatic Solution of Crystal Structure*, University of Göttingen: Germany.
[27] Sheldrick, G. M. (1997). *SHELX97, A Program for Crystal Structure Refinement*, University of Göttingen: Germany.
[28] Frisch, M. J., *et al.* (2003). *Gaussian 03*, Gaussian, Inc., Pittsburgh PA.
[29] Kubicki, M., Borowiak, T., & Antkowiak, W. Z. (1995). *Acta Cryst.*, *C51*, 1173.
[30] Schaefer, T. (1975). *J. Phys. Chem.*, *79*, 1888.
[31] Paul, P., & Bhattacharya, S. (2012). *J. Chem. Sci.*, *124*, 1265.
[32] Phatangare, K., et al. (2013). *J. Chem. Sci.*, *125*, 141.
[33] Chen, K. Y., *et al.* (2014). *J. Lumin.*, *154*, 168.
[34] Chen, K. Y., *et al.* (2014). *J. Chem. Sci.*, *124*, 955.
[35] Nishigaki, S., Yoshioka, H., & Nakatsu, K. (1978). *Acta Cryst.*, *B34*, 875.